

Article

Modeling the Eu(III)-to-Cr(III) Energy Transfer Rates in Luminescent Bimetallic Complexes

Jorge A. A. Coelho ¹, Renaldo T. Moura, Jr. ^{2,3}, Ricardo L. Longo ¹, Oscar L. Malta ^{1,*}
and Albano N. Carneiro Neto ^{4,*} 

¹ Department of Fundamental Chemistry, Federal University of Pernambuco, Recife 50740-560, Brazil

² Department of Chemistry, Southern Methodist University, Dallas, TX 75275-0314, USA

³ Department of Chemistry and Physics, Federal University of Paraíba, Areia 58397-000, Brazil

⁴ Physics Department and CICECO—Aveiro Institute of Materials, University of Aveiro, 3810-193 Aveiro, Portugal

* Correspondence: oscar.malta@ufpe.br (O.L.M.); albanoneto@ua.pt (A.N.C.N.)

Abstract: There is a growing interest in alternatives to lanthanide ion (Ln(III))-based luminescence sensitizing chromophores for in vivo applications, mainly in optical biological windows. Transition metals (M) are relevant candidates as chromophores as they have high absorption rates and emission bands covering a wide range of visible to near-infrared spectrum. However, despite the importance of theoretical models for the design of M–Ln(III) complexes, few contributions have devoted efforts to elucidating the energy transfer (ET) processes between M and Ln(III) ions. In this context, we adapted the intramolecular energy transfer (IET) to calculate, for the first time, the energy transfer rates for M–Ln(III) complexes. A new model was proposed that considers the assistance of phonons in the calculation of ET rates. As an example, the proposed model can estimate the ET rates between Eu(III) and Cr(III) ions in the [CrEuL₃]⁶⁺ complex (where L = 2-[6-[N,N-diethylcarboxamido]pyridin-2-yl]-1,1'-dimethyl-5,5'-methylene-2'-(5-methylpyridin-2-yl)bis[1H-benzimidazole]). The calculated rates (930–1200 s^{−1}) are in excellent agreement with the experimentally available data (750–1200 s^{−1}) when a phonon-assisted energy transfer process is considered. Thus, this proposed model can be useful to predict and explain photophysical properties driven by the energy transfer between Ln(III) ions and transition metals.

Keywords: energy transfer; lanthanide; transition metal; phonon-assisted process; theoretical calculations; heterometallic complexes



Citation: Coelho, J.A.A.; Moura, R.T., Jr.; Longo, R.L.; Malta, O.L.; Carneiro Neto, A.N. Modeling the Eu(III)-to-Cr(III) Energy Transfer Rates in Luminescent Bimetallic Complexes. *Inorganics* **2023**, *11*, 38. <https://doi.org/10.3390/inorganics11010038>

Academic Editor: Valentina Utochnikova

Received: 11 November 2022

Revised: 6 January 2023

Accepted: 9 January 2023

Published: 10 January 2023



Copyright: © 2023 by the authors. Licensee MDPI, Basel, Switzerland. This article is an open access article distributed under the terms and conditions of the Creative Commons Attribution (CC BY) license (<https://creativecommons.org/licenses/by/4.0/>).

1. Introduction

Lanthanide-based compounds are well established in having a wide range of applications, such as in lighting devices [1,2], medicine and bioimaging [3–8], and optical/temperature sensors [9–12]. However, there is also a great interest in alternative chromophores for lanthanide ion (Ln(III))-based luminescence sensitization for near-infrared applications, mainly in biological optical windows [13–15]. Transition metals (M) are often relevant candidates as chromophores because they have high absorption rates and emission bands covering a wide spectral range from visible to infrared [16–18]. Among the transition-metal ions, Cr(III) is a promising example with many applications, including in temperature [19–21] and pressure [22–25] sensing. However, despite the importance of theoretical models for the design of M–Ln(III) complexes, only a few contributions have devoted efforts to elucidate and quantify the energy transfer (ET) processes between M and Ln(III) ions [26,27]. Most approaches describing the efficiency of ET between transition metals and lanthanide ions consist of empirical associations from the difference in the relaxation rates of the sensitizer (donor) in the presence and absence of an acceptor [28–30]. Additionally, to a lesser extent, these approaches perform estimates based on Förster [31] and Dexter [32] models for dipolar (Coulomb) and exchange interactions [17,26,33].

Förster's theory was developed by considering the allowed electric dipole transitions between a donor (D) (or sensitizer) and an acceptor (A) (or activator). However, this approach is not adequate for describing the usual interactions involving lanthanide ions because the 4f-4f transitions are, a priori, forbidden by parity. Furthermore, none of the Förster–Dexter approaches consider the Judd–Ofelt theory for 4f-4f intensities, even though this theory (developed a posteriori) was quite successful in the description of intra-configurational 4f-4f transitions [34]. Indeed, approaches established for Ln–Ln [35–38] and Ligand–Ln [34,39,40] interactions are quite adequate for describing several experimental results [5,41–45]. In this context, there is a gap in theoretical approaches that can quantify ET rates between M–Ln that consider the peculiar properties of both Ln(III) and M centers. Based on Ln–Ln and Ligand–Ln ET approaches, a theoretical framework for describing the ET interactions between M–Ln centers in heterometallic complexes is introduced in this contribution. However, for the M–Ln systems, a new model considering the assistance of phonons in the calculation of ET rates is developed and applied. Estimations of the theoretical ET rates and identification of involved mechanisms are performed for the bimetallic complex [CrEuL₃]⁶⁺ (L = 2-{6-[N,N-diethylcarboxamido]pyridin-2-yl}-1,1'-dimethyl-5,5'-methylene-2'-(5-methylpyridin-2-yl)bis [1H-benzimidazole] [46]. Comparisons with the experimentally determined rates for [CrEuL₃]⁶⁺ are then discussed.

2. Theoretical Methodology

Based on the intramolecular ET model developed by Malta and collaborators [34,39], the determination of M–Ln rates was performed using Equations (1) and (2). These equations were adapted to consider the dipole strength transitions of the metal M (e.g., Cr(III)) and Ln(III), represented by the S_d^M and S_d^{Ln} .

$$W_{d-d} = \frac{2\pi}{\hbar} \frac{S_d^M}{G_M} \frac{S_d^{Ln}}{R_{d-f}^6} F \quad (1)$$

$$W_{d-m} = \frac{2\pi}{\hbar} \frac{S_d^M}{G_M} \sum_{\lambda=2,4,6} \frac{S_\lambda^{Ln}}{(R_{d-f}^{\lambda+2})^2} F \quad (2)$$

where

$$S_d^{Ln} = \frac{2e^2(1-\sigma_1)^2}{(2J+1)} \sum_{\lambda=2,4,6} \Omega_\lambda^{FED} \langle \psi' J' \| U^{(\lambda)} \| \psi J \rangle^2 \quad (3)$$

$$S_\lambda^{Ln} = \frac{(\lambda+1)e^2(1-\sigma_\lambda)^2}{2J+1} \langle r^\lambda \rangle^2 \langle f \| C^{(\lambda)} \| f \rangle^2 \langle \psi' J' \| U^{(\lambda)} \| \psi J \rangle^2 \quad (4)$$

Equation (1) represents the ET rate for the dipole–dipole mechanism and Equation (2) represents the dipole–multipole mechanism. Equations (3) and (4) define S_d^{Ln} and S_λ^{Ln} that represent, respectively, the equivalent dipole and multipole strengths of the lanthanide ion. $\hbar = h/(2\pi)$ is the reduced Planck constant, and $2J+1$ and G_M are the degeneracies of the initial states of the Ln(III) ion and the transition metal, respectively. The term $\langle \psi' J' \| U^{(\lambda)} \| \psi J \rangle$ is the reduced matrix element of the unit tensor operator $U^{(\lambda)}$, operating between states of the Ln(III) ion [47]. The quantity $\langle r^\lambda \rangle$ is the expectation value of the 4f radial wavefunction [48]. The monoelectronic reduced matrix element $\langle f \| C^{(\lambda)} \| f \rangle$ is essentially a 3-j symbol [49,50]. The shielding factors, σ_1 and σ_2 , can be obtained according to the relation given in references [34,51]. For $\lambda = 4$ and 6, the values of σ_λ can be found in reference [48]. The values of each parameter concerning the Ln(III) ion are already implemented in the JOYSpectra web platform [52]. The symbol Ω_λ^{FED} represents the Judd–Ofelt intensity parameter taking into account exclusively the forced electric dipole (FED) contribution. R_{d-f} is the distance between the centroid of the donor and acceptor states, considered in the present work as the distance between the two metallic centers (M–Ln).

The F factor that appears in Equations (1) and (2) represents the density of states between the involved transitions and it is associated with the energy mismatch condition $\Delta = E_D - E_A$ (where E_D and E_A stand for the energy of the donor and acceptor states, respectively). Because the bandwidths of M transitions may vary from the same order of magnitude of Ln(III) transitions ($\sim 10^2 \text{ cm}^{-1}$) to as large as organic ligand bandwidths ($> 10^3 \text{ cm}^{-1}$), the general expression for the F -factor [36,53] is calculated as follows:

$$F = \frac{Y}{(\gamma_D^2 + \gamma_A^2)^{1/2}} \times e^{-(\Delta/\gamma_D)^2 \Gamma} G(\Delta, T) \quad (5)$$

where

$$\Gamma = \left[1 - \frac{1}{1 + (\gamma_D/\gamma_A)^2} \right] \ln 2, \quad Y = \left(\frac{\ln 2}{\pi} \right)^{1/2} \frac{1}{ch} \quad (6)$$

with γ_D and γ_A being, respectively, the bandwidths of the donor and acceptor transitions. c is the speed of light in vacuum and h is the Planck constant.

$G(\Delta, T)$ is the barrier factor associated with the energy difference between the donor and acceptor transitions (Δ). For $\Delta \geq 0$, we have $G(\Delta, T) = 1$, and for $\Delta < 0$, $G(\Delta, T) = e^{\Delta/k_B T}$, in which k_B is the Boltzmann constant and T is the temperature.

At low-resonance conditions (i.e., when $\Delta \gg \gamma_D + \gamma_A$), the participation of phonons in the energy transfer process should not be ruled out. In fact, it can be crucial for bridging the energy gap, mainly in coordination compounds that may present high-energy vibrational modes (e.g., C=N and C=O stretchings). This process is known as phonon-assisted energy transfer [54]. Consequently, the new approach to calculate this F factor considers the form given by Equation (7), which can be obtained from Equation (6.15) in Ref. [54] by truncating the summation at the first term:

$$F' = e^{-(s_D + s_A)} \left[\frac{(s_D + s_A)^N}{N!} \right] \times F(\Delta - N\hbar\bar{\omega}) \times \delta(N, \Delta/\hbar\bar{\omega}) \quad (7)$$

where s_D and s_A are the Huang–Rhys factors for the donor and acceptor electronic states, and N is the number of phonons with average energy $\hbar\bar{\omega}$ necessary to bridge the energy mismatch Δ . The resonance condition is ensured by the Dirac delta function $\delta(N, \Delta/\hbar\bar{\omega})$, while the $F(\Delta - N\hbar\bar{\omega})$ function is the value of F (Equation (5)) with $\Delta = 0$. Therefore, the contribution of $e^{-(\Delta/\gamma_D)^2 \Gamma} G(\Delta, T)$ in Equation (5) is equal to 1.

The dipole strengths S_d^M can be obtained from spectroscopic measurements of the emission lifetime of the transition metal (τ_M) or of its emission rate ($W_M = 1/\tau_M$), in which [39],

$$S_d^M(\tau_M) = \frac{3\hbar}{32\pi^2\sigma^3} \frac{1}{\tau_M} \quad \text{or} \quad S_d^M(W_M) = \frac{3\hbar}{32\pi^2\sigma^3} W_M \quad (8)$$

where σ is the centroid of the M transition in cm^{-1} . Finally, the energy transfer rate (W) is obtained by the sum over W_{d-d} and W_{d-m} rates.

3. Selected Case

The model was used to determine the ET rates between the Eu(III) and Cr(III) ions in the complex $[\text{CrEuL}_3]^{6+}$ ($L = 2\text{-}\{6\text{-}[\text{N,N}\text{-diethylcarboxamido}]\text{pyridin-2-yl}\}\text{-1,1-dimethyl-5,5-methylene-2-(5-methylpyridin-2-yl)bis [1H-benzi-midazole]}$), in which a characteristic Cr(III) emission is observed when the compound is electronically excited at the Eu(III) 5D_0 level, showing the occurrence of Eu(III) \rightarrow Cr(III) ET path, even though the distance (ca. 9.3 Å) between the ions [46] is considerably large.

The experimental ET rate estimated from the Eu(III) lifetimes is about 1000 s^{-1} , obtained as the difference of the inverse of the donor lifetimes ($W = 1/\tau - 1/\tau_0$) in the absence (τ_0) and the presence (τ) of the acceptor [46].

Figure 1 illustrates the structure of the complex obtained from the complex Crystallographic Information File (CIF). Figure 2 shows the electronic levels of the ions involved in the ET process in the complex $[\text{CrEuL}_3]^{6+}$.

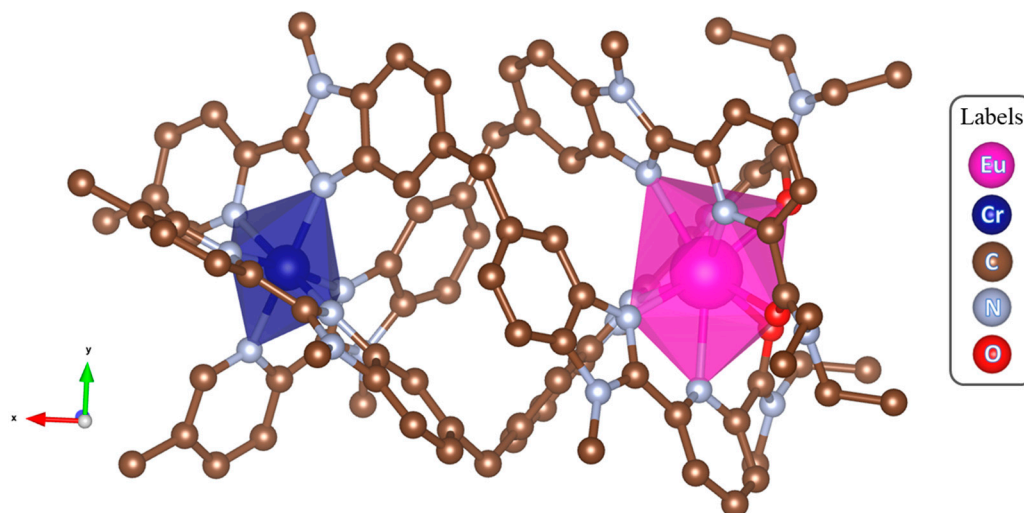


Figure 1. Triple helicate structure of the bimetallic complex $[\text{CrEuL}_3]^{6+}$ highlighting the coordination polyhedrons of Cr and Eu atoms. The geometry was extracted from reference [46] (CCDC code: 176855).

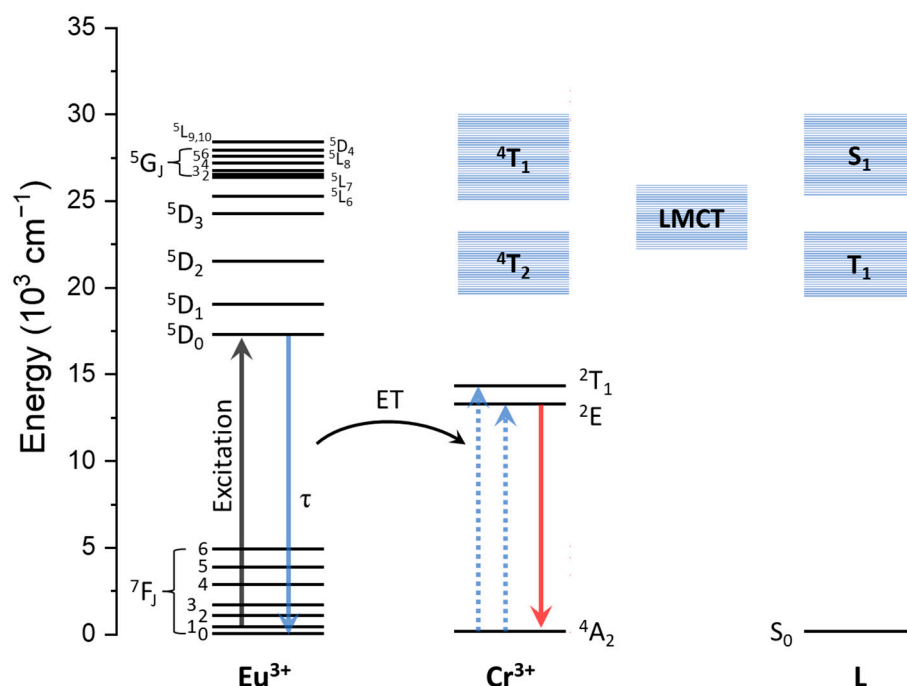


Figure 2. Schematic energy level diagram illustrating the Eu(III), Cr(III), and ligand levels for the $[\text{CrEuL}_3]^{6+}$ complex. The blue solid arrow represents the Eu(III) decay (τ is the decay lifetime), while the upward dashed arrows, at the Cr(III) side, represent ${}^2\text{E} \leftarrow {}^4\text{A}_2$ and ${}^2\text{T}_1 \leftarrow {}^4\text{A}_2$ excitation through the ET process. The Cr(III) ${}^2\text{E} \rightarrow {}^4\text{A}_2$ emission is denoted by a red arrow. The upper levels of Eu(III) (from ${}^5\text{D}_1$ to ${}^5\text{L}_{10}$), Cr(III) (${}^4\text{T}_2$ and ${}^4\text{T}_1$), and ligand states (T_1 and S_1), as well as the ligand-to-metal charge transfer (LMCT) state are included for completeness as they do not participate in the energy transfer process because they are far from the excitation at the Eu(III) ${}^5\text{D}_0$ level.

All spectroscopic data from the literature [46,55] were extracted using the WebPlotDigitizer online tool [56]. From the Eu(III) side, the intensity parameters $\Omega_\lambda^{\text{FED}}$ were determined

utilizing the crystallographic structure of the $[\text{CrEuL}_3]^{6+}$ complex as the input data in the JOYSpectra web platform [52] and the $\text{Eu(III)} \ ^5\text{D}_0 \rightarrow \ ^7\text{F}_J$ ($J = 2, 4,$ and 6) transitions were considered as the donor states.

The theoretical model needs experimental data from the acceptor and donor transitions. Cantuel et al. [46] reported both the emission spectrum of the Eu(III) and the absorption spectrum of the Cr(III) in $[\text{CrEuL}_3]^{6+}$. However, it is not possible to define the peaks and bandwidths of the Cr(III) states (^2E and $^2\text{T}_1$) in the absorption spectrum, the necessary quantities for calculating the F factor (Equation (5)). To circumvent this issue, we employed spectroscopic data from a similar complex available in the literature [55].

Golesorkhi and collaborators [55] reported triple helicate complexes with three metallic centers (two Cr(III) and one Ln(III)), which exhibit similar coordination environments and ligand-field strengths to the $[\text{CrEuL}_3]^{6+}$ target complex. Comparing the data from the $[\text{CrLnCr}(\text{bpb-bzimpy})_3]^{9+}$ complexes [55] with the $[\text{CrEuL}_3]^{6+}$ [46], it is also observed that there is a similarity in the Cr(III) electronic levels. Therefore, the data from the literature [55] were used as a reference for estimating the necessary parameters in the energy transfer rate calculations with Equations (1) and (2).

The theoretical ET rates were estimated with two different procedures: (i) by the summation of the individual ET rates, considering the Cr(III) transitions ($^2\text{E} \leftarrow ^4\text{A}_2$ and $^2\text{T}_1 \leftarrow ^4\text{A}_2$) separately, and (ii) by considering these two Cr(III) transitions together in an envelope fitted by a Gaussian function, leading to a single ET rate.

Figure 3 shows the $\text{Cr(III)} \ ^2\text{E}, ^2\text{T}_1 \leftarrow ^4\text{A}_2$ transitions as well as the envelope including both transitions for the $[\text{CrErCr}(\text{bpb-bzimpy})_3]^{9+}$ complex [55].

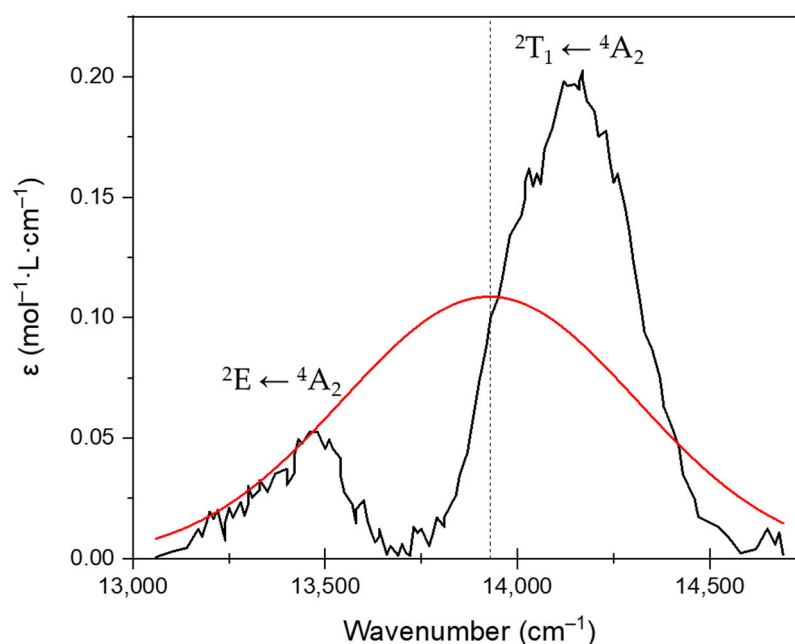


Figure 3. Absorption peaks of $\text{Cr(III)} \ ^2\text{E} \leftarrow ^4\text{A}_2$ and $^2\text{T}_1 \leftarrow ^4\text{A}_2$ transitions (black lines) for the $[\text{CrErCr}(\text{bpb-bzimpy})_3]^{9+}$ complex. The red curve is the envelope involving these two transitions. Adapted with permission from [55].

4. Results and Discussion

4.1. Multipolar Energy Transfer Rates

To calculate the dipole–dipole ET rate, it is necessary to obtain the intensity parameters of the forced electric dipole mechanism ($\Omega_\lambda^{\text{FED}}, \lambda = 2, 4, 6$) based on the original Judd–Ofelt theory [57,58]. These values were estimated using the crystallographic structure of the complex as the input data in the JOYSpectra web platform [52]. The calculated values, in units of 10^{-20} cm^2 , are $\Omega_\lambda^{\text{FED}} = 0.269, 0.222,$ and 0.353 for $\lambda = 2, 4, 6$, respectively.

The F factor (Equation (5)) was obtained using the bandwidth $\gamma_D \approx 200 \text{ cm}^{-1}$ and energy barycenters $E(^5D_0 \rightarrow ^7F_\lambda) \approx 16,166, 14,400, \text{ and } 12,386 \text{ cm}^{-1}$ for $\lambda = 2, 4, 6$, respectively [46,47]. The bandwidths (γ_A) of Cr(III) are 236 and 390 cm^{-1} for the $^2E \leftarrow ^4A_2$ and $^2T_1 \leftarrow ^4A_2$ transitions, respectively. The dipole strength $S_d^M(\tau_M) \approx 2 \times 10^{-38} \text{ esu}^2 \cdot \text{cm}^2$ was estimated from the Cr(III) emission lifetime at room temperature (Equation (8)).

Considering the ET from Eu(III) to individual Cr(III) transitions ($^2E \leftarrow ^4A_2$ and $^2T_1 \leftarrow ^4A_2$), two set of ET pathways are obtained: Eu(III) [$^5D_0 \rightarrow ^7F_J$] \rightarrow Cr(III) [$^2E \leftarrow ^4A_2$] and Eu(III) [$^5D_0 \rightarrow ^7F_J$] \rightarrow Cr(III) [$^2T_1 \leftarrow ^4A_2$]. Table 1 presents the values of the F factor and the ET rates for each pathway (pathways 1–3 involve the 2E , whilst pathways 4–6 involve the 2T_1 state).

Table 1. Theoretical ET rates at room temperature for the $[\text{CrEuL}_3]^{6+}$ complex. The donor–acceptor distance is $R_{d-f} = 9.3$. The values were calculated using $S_d^M(\tau_M) = 2 \times 10^{-38} \text{ esu}^2 \cdot \text{cm}^2$. Δ is the energy difference between the donor and acceptor transitions. W is the sum of W_{d-d} and W_{d-m} in the same pathway, and the total rate W_{total} is the rate obtained by summing all pathways.

Pathway	Donor	Acceptor	$\Delta \text{ (cm}^{-1}\text{)}$	$F \text{ (erg}^{-1}\text{)}$	$W_{d-d} \text{ (s}^{-1}\text{)}$	$W_{d-m} \text{ (s}^{-1}\text{)}$	$W \text{ (s}^{-1}\text{)}$
1	$^5D_0 \rightarrow ^7F_2$	$^2E \leftarrow ^4A_2$	2748	1×10^{-11}	1×10^{-22}	3×10^{-20}	3×10^{-20}
2	$^5D_0 \rightarrow ^7F_4$	$^2E \leftarrow ^4A_2$	982	7×10^9	4×10^{-2}	3×10^{-3}	4×10^{-2}
3	$^5D_0 \rightarrow ^7F_6$	$^2E \leftarrow ^4A_2$	−1032	2×10^7	3×10^{-5}	5×10^{-10}	3×10^{-5}
4	$^5D_0 \rightarrow ^7F_2$	$^2T_1 \leftarrow ^4A_2$	2026	2×10^6	7×10^{-6}	3×10^{-3}	3×10^{-3}
5	$^5D_0 \rightarrow ^7F_4$	$^2T_1 \leftarrow ^4A_2$	260	4×10^{12}	20	1	21
6	$^5D_0 \rightarrow ^7F_6$	$^2T_1 \leftarrow ^4A_2$	−1754	2×10^4	1×10^{-8}	2×10^{-13}	1×10^{-8}
$W_{\text{total}} = \sum_{i=1}^6 W_i =$							21

It can be noticed that the donor Eu(III) $^5D_0 \rightarrow ^7F_4$ transition is more resonant with the Cr(III) acceptor transitions, mainly with the $^2T_1 \leftarrow ^4A_2$ one ($\Delta = 260 \text{ cm}^{-1}$, pathway 5 in Table 1), providing high values of F that could result in significant ET rates. However, the rates of pathways 2 and 5 (Table 1) are very low and very dissonant with the experimental ET rate ($\sim 1000 \text{ s}^{-1}$). This is because the selection rules on J quantum number, in which $\langle ^5D_0 || U^{(2)} || ^7F_4 \rangle^2 = 0$, being the dipole–quadrupole interaction equals to zero (first term of the summation in Equation (2)). Consequently, despite being very resonant, the $^5D_0 \rightarrow ^7F_4$ transition has only the dipole–hexadecapole (2^4 -pole) contributing to W_{d-m} , which is orders of magnitude smaller due to the dependence on the donor–acceptor distance, $W_{d-m} \propto R_{d-f}^{-12}$.

In cases of ligand-to-Ln(III) intramolecular energy transfer, significant ET rates are obtained with a typical energy gap around 2000 cm^{-1} between the transitions of the ligands and the lanthanide ions, because the bandwidths of the ligand states are of the order of or larger than the energy gap, offering a better resonance situation that results in F factors of $\sim 10^{11} - 10^{12} \text{ erg}^{-1}$ [59].

For pathways 1 and 4 in Table 1, the bandwidths of both species (donor and acceptor) are smaller than the energy gap Δ . As a result, the F factors are very small and determinants for the negligible ET rates obtained. This situation is different when calculating the Eu(III) \rightarrow Cr(III) ET rate considering the envelope of $^2E \leftarrow ^4A_2$ and $^2T_1 \leftarrow ^4A_2$ transitions (see Table 2) as the entire spectral range in Figure 3. The bandwidth of the envelope has the centroid at 13930 cm^{-1} with a bandwidth of $\sim 900 \text{ cm}^{-1}$. With a larger Cr(III) bandwidth (about half the energy gap), the F for the $^5D_0 \rightarrow ^7F_2$ transition (pathway 1 in Table 2) assumes values of $\sim 10^{10} \text{ erg}^{-1}$ and the ET rate for the dipole–multipole mechanism (W_{d-m}) becomes dominant, although it is less resonant than the $^5D_0 \rightarrow ^7F_4$ transition, as displayed for the values of Δ in Table 2. This occurs because the contribution of the dipole–quadrupole mechanism for the $^5D_0 \rightarrow ^7F_2$ transition is non-zero due to the selection rule on J quantum number, namely, $\langle ^5D_0 || U^{(2)} || ^7F_4 \rangle^2 = 0.0032$.

Table 2. Theoretical ET rates at room temperature for the $[\text{CrEuL}_3]^{6+}$ complex considering the acceptor transition as the barycenter of $\text{Cr(III)} \ ^2\text{E}, \ ^2\text{T}_1 \leftarrow \ ^4\text{A}_2$ transitions (envelope). $R_{\text{d-f}} = 9.3$. W is the sum of $W_{\text{d-d}}$ and $W_{\text{d-m}}$ in the same pathway and the total rate W_{total} is the sum over of all pathways rates.

Pathway	Donor	Δ (cm ⁻¹)	F (erg ⁻¹)	$W_{\text{d-d}}$ (s ⁻¹)	$W_{\text{d-m}}$ (s ⁻¹)	W (s ⁻¹)
1	$^5\text{D}_0 \rightarrow ^7\text{F}_2$	2239	4×10^{10}	4×10^{-1}	98	98
2	$^5\text{D}_0 \rightarrow ^7\text{F}_4$	470	2×10^{12}	11	8×10^{-1}	11
3	$^5\text{D}_0 \rightarrow ^7\text{F}_6$	-1541	2×10^8	2×10^{-4}	4×10^{-9}	2×10^{-4}
$W_{\text{total}} = \sum_{i=1}^3 W_i =$						109

The calculated ET rate considering the envelope of the Cr(III) transitions ($W_{\text{total}} = 109 \text{ s}^{-1}$) is one order of magnitude lower than the experimental rate ($\sim 1000 \text{ s}^{-1}$). This underestimation is due to a weak resonance between the donor and acceptor transitions (large values of Δ for the $^5\text{D}_0 \rightarrow ^7\text{F}_2$ donor transition). Hence, the calculations for the $[\text{EuCrL}_3]^{6+}$ without considering a phonon-assisted energy transfer process, as displayed in Tables 1 and 2, are not adequate to produce reasonable values of ET rates.

4.2. Exchange Energy Transfer Rates

The model can also include the contribution of the exchange mechanism in the Eu(III) \rightarrow Cr(III) ET process. This mechanism strongly depends on the overlap integral between the valence orbitals of the donor and the acceptor ions [32,36]. Thus, for a distance of $R_{\text{d-f}} = 9.3 \text{ \AA}$ for the $[\text{EuCrL}_3]^{6+}$ complex, the value of the d-f overlap integral (ρ) is indeed negligible (the highlighted point in Figure 4 indicates $\rho \approx 10^{-10}$ for $R_{\text{d-f}} = 9.3 \text{ \AA}$), and this accounts for the vanishing value of the rate by the exchange mechanism. The Cr(III)–Eu(III) overlap integrals were estimated according to the procedure in Ref. [51].

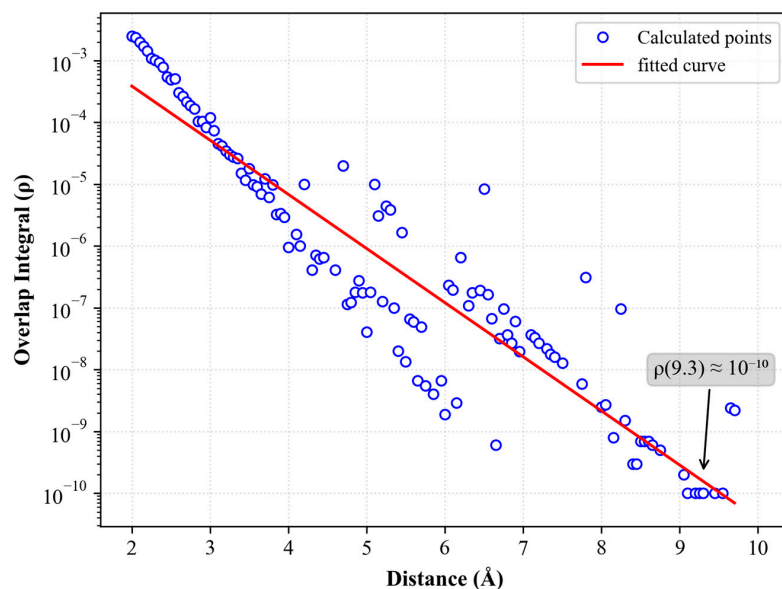


Figure 4. Calculated values and the linear fit of the overlap integral (ρ) between the valence orbitals of Cr(III) and Eu(III) ions as a function of the distance between the metal ions, $R_{\text{d-f}}$, obtained with the procedure described in reference [51]. The highlighted point indicates a value of $\rho \approx 10^{-10}$ when $R_{\text{d-f}} = 9.3 \text{ \AA}$.

4.3. Phonon-Assisted Energy Transfer

As the energy transfer process must ensure energy conservation, it is reasonable that the process could be assisted by phonons, bridging the energy gap between the donor and

acceptor transitions [60]. In this case, an expression for the F' factor (Equation (7)) based on the Miyakawa–Dexter approach [54] was employed, which involves the Huang–Rhys factors associated with the donor and acceptor transitions (s_D and s_A , respectively), as well as the average phonon energy ($\hbar\bar{\omega}$) and number of phonons (N) involved in the ET process.

The Huang–Rhys factors for lanthanide ions are of the order of $s_D \sim 10^{-2}$ due to the weak vibronic coupling [61–65]. For transition metals, the Huang–Rhys factors are usually in the intermediate coupling range (values between one and five). Indeed, the transitions involving the 2E and 2T_1 states are in the lower limit of the intermediate vibronic coupling range, presenting values around one [66,67].

To proceed with the phonon-assisted energy transfer rate calculations, the F' factor (Equation (7)) was calculated for the typical ranges of the Huang–Rhys factors, considering the vibronic couplings involved. In the case of the Eu(III) donor transitions, the s_D is in the [0.01–0.10] range, while for the Cr(III) acceptor transitions, s_A was considered to be within the [0.1–1.2] range. The average phonon energies were considered to be between 1000 and 1300 cm^{-1} , which matches with the C=N stretching modes of aliphatic amines (1020–1250 cm^{-1}) and aromatic imines (1250–1340 cm^{-1}) [68], indicating that the vibrational modes of the coordinated nitrogen atoms have an important role in the phonon-assisted energy transfer. In addition, this suggests the participation of two phonons in the ET process, which is feasible. These values of the average phonon energies are consistent with the single-configurational coordinate model applied to related triple-helical complexes, $\text{Na}_3[\text{Ln}(\text{dpa})_3] \cdot 13\text{H}_2\text{O}$, which employed a phonon energy of 1200 cm^{-1} [69]. However, this same work employed a Huang–Rhys factor of two to estimate the energy transfer rates, which could be considered too large for Ln(III) complexes.

Figure 5 displays the surface of the ET rates as a function of the Huang–Rhys factors, considering that two phonons are bridging the energy gap. It is noteworthy that the ET rates change only slightly with s_D , while they are strongly dependent on the values of s_A . Accordingly, to reproduce the experimental ET rate of 1000 s^{-1} , s_A should acquire values close to one, which is consistent with the lower limit of the vibronic couplings of the Cr(III) acceptor transitions [66,67]. To better illustrate these results, Table 3 presents a range of s_A and s_D extracted from the surface in Figure 5, resulting in total rates of around 1000 s^{-1} .

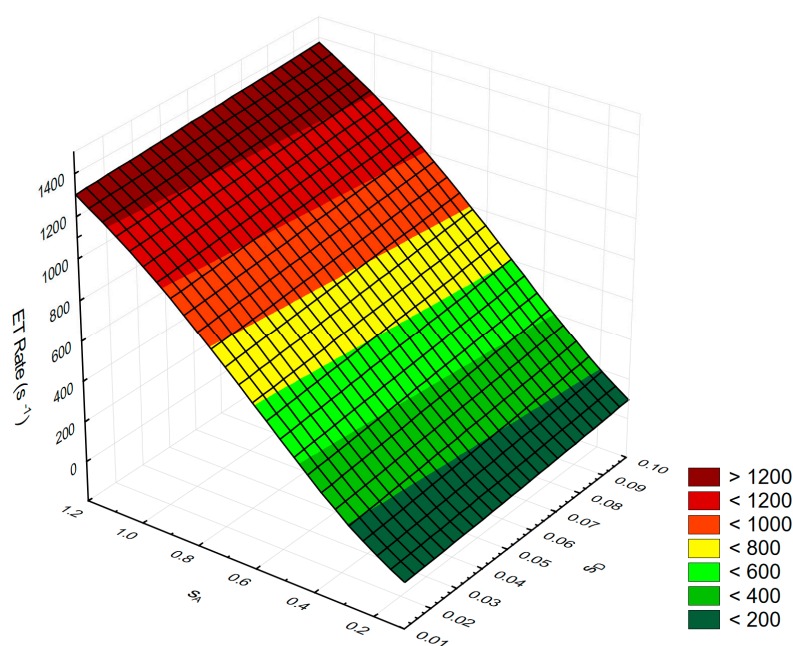


Figure 5. ET rate $\text{Eu(III)} \rightarrow \text{Cr(III)}$ as a function of the Huang–Rhys factors and considering the participation of 2 phonons in the ET process. s_A and s_D are the Huang–Rhys factors for the involved transitions of the Cr(III) and Eu(III) ions, respectively.

Table 3. Phonon-assisted energy transfer rates (W) and their mechanisms' contributions (W_{d-d} and W_{d-m}). The average phonon energy $\hbar\bar{\omega} = 1120 \text{ cm}^{-1}$ is considered in a two-phonon process. s_D and s_A are the Huang–Rhys factors for the donor and acceptor, respectively. F' is the phonon-assisted spectral overlap factor (Equation (7)).

s_D	s_A	F' ($10^{11} \cdot \text{erg}^{-1}$)	W_{d-d} (s^{-1})	W_{d-m} (s^{-1})	W (s^{-1})
0.01	0.85	4.1	3.4	927.6	931.0
0.01	0.90	4.3	3.6	987.9	991.5
0.01	0.95	4.6	3.8	1046.8	1050.6
0.01	1.00	4.8	4.0	1101.2	1105.2
0.04	0.85	4.2	3.5	964.1	967.6
0.04	0.90	4.5	3.8	1023.0	1026.8
0.04	0.95	4.7	4.0	1079.4	1083.4
0.04	1.00	4.9	4.2	1133.0	1137.2
0.08	0.85	4.4	3.7	1011.4	1015.1
0.08	0.90	4.7	3.9	1068.3	1072.2
0.08	0.95	4.9	4.1	1122.5	1126.6
0.08	1.00	5.1	4.3	1174.0	1178.3
0.10	0.85	4.5	3.8	1034.5	1038.3
0.10	0.90	4.8	4.0	1090.3	1094.3
0.10	0.95	5.0	4.2	1143.4	1147.6
0.10	1.00	5.2	4.4	1193.7	1198.1

The results in Table 3 emphasize the weak influence of s_D on the energy transfer process. For example, considering fixed values of s_A , the ET rates vary between ca. 930 and 1070 s^{-1} when the s_D increases 10 times (from 0.01 to 0.10). In contrast, when the s_A is slightly increased by 1.18 times (from 0.85 to 1.00), the ET rates significantly vary between 1600 and 1740 s^{-1} . This indicates that the phonon-assisted energy transfer process has a dominant contribution from the coupling of the Cr(III) states with the vibrational modes of the complex. As mentioned, this process should have a significant participation in the N–C vibrational modes in the coordination polyhedron.

In the case of Ln(III)–Ln(III) interaction, the efficiency of the energy transfer has a strong dependence on the resonance of the donor and acceptor states, mainly due to the narrow bandwidths of the transitions [37] and the weak vibronic coupling, expressed by the small Huang–Rhys factors [61–65].

Regarding the ET mechanisms, Ward [26] reported ET rates for M–Ln(III) systems with large intermetallic distances and suggested that the Dexter mechanism should be the most likely ET one (exchange) because the Ln(III) 4f–4f transitions are forbidden and the long M···Ln(III) distances are unfavorable for the dipole–dipole (Förster) mechanism. However, the present work indicates that multipolar mechanisms can be dominant in the ET process.

The model developed here considers the Judd–Ofelt theory, in which the forbidden character of 4f–4f transitions is treated through the forced electric dipole mechanism. Therefore, the model can predict that the multipolar mechanisms play a dominant role in energy transfer for the $[\text{CrEuL}_3]^{6+}$ complex (see Table 3).

At this point, a comment concerning the cases of Eu(III)–Cr(III), Ln(III)–Ln(III), and organic ligand–Ln(III) non-radiative energy transfer should be made. In the latter case, the bandwidths of the donor (e.g., ligands, γ_D) and the acceptor (e.g., Ln(III), γ_A) are extremely different, with γ_D being much larger than γ_A , i.e., $\gamma_D \gg \gamma_A$. Thus, in the evaluation of the energy mismatch factor (or spectral overlap) in the F factor, provided the organic ligand bandwidth is used, the ligand vibrational band structure is encompassed. An approximate form of Equation (5) has been successfully employed for this case. For the ET between lanthanide ions, Ln(III)–Ln(III), the donor and acceptor bandwidths are similar, $\gamma_D \approx \gamma_A$, and very small due to the very weak vibronic couplings and the features of the 4f–4f transitions. Thus, the complete form of the F factor in Equation (5) has been used. On the other hand, d–d transitions in transition-metal complexes have a considerable vibronic coupling contribution to their intensities, and they are not as large as organic ligand bands.

This justifies the use of Equation (7) in terms of the Huang–Rhys factors (in the intermediate or strong vibronic coupling regimes) and an average promoting vibrational frequency.

The assumptions of the present model come from the Judd–Ofelt theory (for the calculation the dipole strengths S_d^{Ln}), which considers that the intra-configurational energy differences, $\Delta E(4f^N, 4f^{N-1}nl)$, are much smaller than the inter-configurational energy differences, $\Delta E(4f^N)$, i.e., $\Delta E(4f^N, 4f^{N-1}nl) \ll \Delta E(4f^N, 4f^{N-1}nl)$ [70], and from the shielding factors σ_1 and σ_2 , whose values are obtained from quantum chemistry calculations for diatomic systems (e.g., Eu–O and Eu–N) [51]. However, even with these approximations, the model can reproduce the values of energy transfer rates in great accordance with the experimental ones.

5. Conclusions

A theoretical model to calculate the ET rates between a lanthanide ion and a transition metal is introduced. The $[\text{CrEuL}_3]^{6+}$ complex was chosen as a case study and the Eu–Cr energy transfer rates, when considered a phonon-assisted process, agree with the experimental ones. The theoretical rates are around $930\text{--}1200\text{ s}^{-1}$, with a predominance of the dipole–multipole mechanism (W_{d-m}) for an Eu–Cr distance of 9.3 \AA , which is in excellent agreement with the experimental value of ca. 1000 s^{-1} .

The sensitivity of the estimated rates to the Huang–Rhys factors was analyzed within the range of $s_D = [0.01\text{ to }0.1]$ for Eu(III) and $s_A = [0.1\text{ to }1.2]$ for Cr(III), and the results show that the latter, s_A , has a strong effect on the ET rates. Indeed, the calculated rates agree with the experimental value when the Huang–Rhys factor for the acceptor (Cr(III)) is within $s_A = [0.85\text{ to }1.00]$, which is consistent with the lower limit of the vibronic couplings in similar Cr(III) complexes. These calculations of the ET rates using the phonon-assisted model considered a two-phonon process to bridge the energy mismatch, which is consistent with C=N vibrational modes ($\hbar\bar{\omega} \approx 1000\text{--}1200\text{ cm}^{-1}$) near the metal centers.

The proposed model can be useful for predicting and explaining photophysical properties driven by energy transfer between Ln(III) and transition metals, quantifying the contributions of each mechanism and the factors that may optimize energy transfer rates and efficiencies.

As the first study involving the calculation of theoretical Ln–M ET rates that considers the Judd–Ofelt theory and the phonon-assisted process, we hope to motivate more experimental works focused on the determination of energy transfer rates between lanthanides and transition metals for the design of new luminescent materials.

Author Contributions: J.A.A.C.: Conceptualization, Methodology, Software, Validation, Formal analysis, Investigation, Data Curation, Writing—Original Draft, and Writing—Review and Editing. R.T.M.J.: Conceptualization and Writing—Review and Editing. R.L.L.: Conceptualization and Writing—Review and Editing. O.L.M.: Conceptualization, Methodology, Formal analysis, Writing—Original Draft, Writing—Review and Editing, and Supervision. A.N.C.N.: Conceptualization, Methodology, Software, Validation, Formal analysis, Investigation, Data Curation, Writing—Original Draft, Writing—Review and Editing, and Supervision. All authors have read and agreed to the published version of the manuscript.

Funding: This work was funded by the Public Call n. 03 *Produtividade em Pesquisa* PROPESQ/PRPG/UFPB project number PVN13305-2020, and PROPESQ/CNPq/UFPB PIN11132-2019. R.L.L. is grateful for the partial financial support under grants Pronex APQ-0675-1.06/14, INCT-NANOMARCS APQ-0549-1.06/17, APQ-1007-1.06/15, and CNPq-PQ fellowship (Proc. 309177/2018-9). R.T.M.J. thanks the SMU's Center for Scientific Computing for providing generous computational resources. This work was developed within the scope of the projects CICECO-Aveiro Institute of Materials, UIDB/50011/2020, UIDP/50011/2020 & LA/P/0006/2020, The Shape of Water (PTDC/NAN-PRO/3881/2020), and LogicALL (PTDC/CTM-CTM/0340/2021) financed by national funds through the FCT/MCTES (PIDDAC).

Data Availability Statement: Not applicable.

Acknowledgments: The authors thank the reviewers' evaluations of the manuscript, especially the comments and suggestions by Reviewer #4.

Conflicts of Interest: The authors declare no conflict of interest.

References

1. De Bettencourt-Dias, A. Lanthanide-based emitting materials in light-emitting diodes. *Dalton Trans.* **2007**, *22*, 2229–2241. [[CrossRef](#)]
2. Fang, M.; Neto, A.N.C.; Fu, L.; Ferreira, R.A.S.; deZeaBermudez, V.; Carlos, L.D. A Hybrid Materials Approach for Fabricating Efficient WLEDs Based on Di-Ureasils Doped with Carbon Dots and a Europium Complex. *Adv. Mater. Technol.* **2021**, *7*, 2100727. [[CrossRef](#)]
3. Ou, X.; Qin, X.; Huang, B.; Zan, J.; Wu, Q.; Hong, Z.; Xie, L.; Bian, H.; Yi, Z.; Chen, X.; et al. High-resolution X-ray luminescence extension imaging. *Nature* **2021**, *590*, 410–415. [[CrossRef](#)]
4. Neto, A.N.C.; Malta, O.L. Glowing nanocrystals enable 3D X-ray imaging. *Nature* **2021**, *590*, 396–397. [[CrossRef](#)]
5. Piñol, R.; Zeler, J.; Brites, C.D.S.; Gu, Y.; Téllez, P.; Neto, A.N.C.; Da Silva, T.E.; Moreno-Loshuertos, R.; Fernandez-Silva, P.; Gallego, A.I.; et al. Real-Time Intracellular Temperature Imaging Using Lanthanide-Bearing Polymeric Micelles. *Nano Lett.* **2020**, *20*, 6466–6472. [[CrossRef](#)]
6. Cotruvo, J.A. The Chemistry of Lanthanides in Biology: Recent Discoveries, Emerging Principles, and Technological Applications. *ACS Central Sci.* **2019**, *5*, 1496–1506. [[CrossRef](#)]
7. Faulkner, S.; Blackburn, O.A. The Chemistry of Lanthanide MRI Contrast Agents. In *The Chemistry of Molecular Imaging*; John Wiley & Sons, Inc: Hoboken, NJ, USA, 2014; pp. 179–197.
8. Perrier, M.; Gallud, A.; Ayadi, A.; Kennouche, S.; Porredon, C.; Gary-Bobo, M.; Larionova, J.; Goze-Bac, C.; Zanca, M.; Garcia, M.; et al. Investigation of cyano-bridged coordination nanoparticles $Gd^{3+}/[Fe(CN)_6]^{3-}$ /d-mannitol as T_1 -weighted MRI contrast agents. *Nanoscale* **2015**, *7*, 11899–11903. [[CrossRef](#)]
9. Ramalho, J.F.; Neto, A.N.C.; Carlos, L.D.; André, P.S.; Ferreira, R.A. Lanthanides for the new generation of optical sensing and Internet of Things. In *Handbook on the Physics and Chemistry of Rare Earths*; Bünzli, J.-C.G., Pecharsky, V.K., Eds.; Elsevier: Amsterdam, The Netherlands, 2022; pp. 31–128. [[CrossRef](#)]
10. Brites, C.D.S.; Millán, A.; Carlos, L.D. Lanthanides in Luminescent Thermometry. In *Handbook on the Physics and Chemistry of Rare Earths*; Bünzli, J.-C.G., Pecharsky, V.K., Eds.; Elsevier: Amsterdam, The Netherlands, 2016; Volume 49, pp. 339–427.
11. Salerno, E.V.; Neto, A.N.C.; Eliseeva, S.V.; Hernández-Rodríguez, M.A.; Lutter, J.C.; Lathion, T.; Kampf, J.W.; Petoud, S.; Carlos, L.D.; Pecoraro, V.L. Tunable Optical Molecular Thermometers Based on Metallocrowns. *J. Am. Chem. Soc.* **2022**, *144*, 18259–18271. [[CrossRef](#)]
12. De Souza, K.M.N.; Silva, R.N.; Silva, J.A.B.; Brites, C.D.S.; Francis, B.; Ferreira, R.A.S.; Carlos, L.D.; Longo, R.L. Novel and High-Sensitive Primary and Self-Referencing Thermometers Based on the Excitation Spectra of Lanthanide Ions. *Adv. Opt. Mater.* **2022**, *10*, 2200770. [[CrossRef](#)]
13. Sun, L.; Shi, L. Lanthanides: Near-Infrared Materials. In *Encyclopedia of Inorganic and Bioinorganic Chemistry*; John Wiley & Sons, Ltd.: Chichester, UK, 2012.
14. Cho, U.; Chen, J.K. Lanthanide-Based Optical Probes of Biological Systems. *Cell Chem. Biol.* **2020**, *27*, 921–936. [[CrossRef](#)]
15. Rocha, U.; Kumar, K.U.; Jacinto, C.; Villa, I.; Sanz-Rodríguez, F.; del Carmen Iglesias de la Cruz, M.; Juarranz, A.; Carrasco, E.; van Veggel, F.C.J.M.; Bovero, E.; et al. Neodymium-Doped LaF_3 Nanoparticles for Fluorescence Bioimaging in the Second Biological Window. *Small* **2013**, *10*, 1141–1154. [[CrossRef](#)]
16. Sábio, R.M.; Santagneli, S.H.; Gressier, M.; Caiut, J.M.A.; Pazin, W.M.; Leite, I.S.; Inada, N.M.; da Silva, R.R.; Ribeiro, S.J.L.; Menu, M.-J. Luminescent nanohybrids based on silica and silylated Ru(II)—Yb(III) heterobinuclear complex: New tools for biological media analysis. *Nanotechnology* **2019**, *31*, 085709. [[CrossRef](#)]
17. Ward, M.D. Transition-metal sensitised near-infrared luminescence from lanthanides in d–f heteronuclear arrays. *Coord. Chem. Rev.* **2007**, *251*, 1663–1677. [[CrossRef](#)]
18. Chen, F.-F.; Chen, Z.-Q.; Bian, Z.-Q.; Huang, C.-H. Sensitized luminescence from lanthanides in d–f bimetallic complexes. *Coord. Chem. Rev.* **2010**, *254*, 991–1010. [[CrossRef](#)]
19. Back, M.; Ueda, J.; Nambu, H.; Fujita, M.; Yamamoto, A.; Yoshida, H.; Tanaka, H.; Brik, M.G.; Tanabe, S. Boltzmann Thermometry in Cr^{3+} -Doped Ga_2O_3 Polymorphs: The Structure Matters! *Adv. Opt. Mater.* **2021**, *9*, 2100033. [[CrossRef](#)]
20. Malysa, B.; Meijerink, A.; Jüstel, T. Temperature dependent Cr^{3+} photoluminescence in garnets of the type $X_3Sc_2Ga_3O_{12}$ ($X = Lu, Y, Gd, La$). *J. Lumin.* **2018**, *202*, 523–531. [[CrossRef](#)]
21. Back, M.; Ueda, J.; Brik, M.G.; Tanabe, S. Pushing the Limit of Boltzmann Distribution in Cr^{3+} -Doped $CaHfO_3$ for Cryogenic Thermometry. *ACS Appl. Mater. Interfaces* **2020**, *12*, 38325–38332. [[CrossRef](#)]
22. Back, M.; Ueda, J.; Hua, H.; Tanabe, S. Predicting the Optical Pressure Sensitivity of ${}^2E \rightarrow {}^4A_2$ Spin-Flip Transition in Cr^{3+} -Doped Crystals. *Chem. Mater.* **2021**, *33*, 3379–3385. [[CrossRef](#)]
23. Shen, Y.; Grinberg, M.; Barzowska, J.; Bray, K.; Hanuza, J.; Dereñ, P. The effect of pressure on luminescence properties of Cr^{3+} ions in $LiSc(WO_4)_2$ crystals—Part I: Pressure dependent emission lineshape. *J. Lumin.* **2006**, *116*, 1–14. [[CrossRef](#)]

24. Grinberg, M.; Barzowska, J.; Shen, Y.; Bray, K.; Hanuza, J.; Dereń, P. The effect of pressure on luminescence properties of Cr³⁺ ions in LiSc(WO₄)₂ crystals—Part II: Pressure- and temperature-dependent luminescence kinetics. *J. Lumin.* **2006**, *116*, 15–27. [[CrossRef](#)]
25. Szymczak, M.; Woźny, P.; Runowski, M.; Pieprz, M.; Lavín, V.; Marciniak, L. Temperature invariant ratiometric luminescence manometer based on Cr³⁺ ions emission. *Chem. Eng. J.* **2023**, *453*, 139632. [[CrossRef](#)]
26. Ward, M.D. Mechanisms of sensitization of lanthanide(III)-based luminescence in transition metal/lanthanide and anthracene/lanthanide dyads. *Coord. Chem. Rev.* **2010**, *254*, 2634–2642. [[CrossRef](#)]
27. Lazarides, T.; Davies, G.M.; Adams, H.; Sabatini, C.; Barigelletti, F.; Barbieri, A.; Pope, S.J.A.; Faulkner, S.; Ward, M.D. Ligand-field excited states of hexacyanochromate and hexacyanocobaltate as sensitizers for near-infrared luminescence from Nd(III) and Yb(III) in cyanide-bridged d–f assemblies. *Photochem. Photobiol. Sci.* **2007**, *6*, 1152–1157. [[CrossRef](#)]
28. Chen, F.-F.; Wei, H.-B.; Bian, Z.-Q.; Liu, Z.-W.; Ma, E.; Chen, Z.-N.; Huang, C.-H. Sensitized Near-Infrared Emission from Ir^{III}-Ln^{III} (Ln = Nd, Yb, Er) Bimetallic Complexes with a (N[^]O)(N[^]O) Bridging Ligand. *Organometallics* **2014**, *33*, 3275–3282. [[CrossRef](#)]
29. Crowston, B.J.; Shipp, J.D.; Chekulaev, D.; McKenzie, L.K.; Jones, C.; Weinstein, J.A.; Meijer, A.J.H.; Bryant, H.E.; Natrajan, L.; Woodward, A.; et al. Heteronuclear d–d and d–f Ru(II)/M complexes [M = Gd(III), Yb(III), Nd(III), Zn(II) or Mn(II)] of ligands combining phenanthroline and aminocarboxylate binding sites: Combined relaxivity, cell imaging and photophysical studies. *Dalton Trans.* **2019**, *48*, 6132–6152. [[CrossRef](#)]
30. Singaravadivel, S.; Velayudham, M.; Babu, E.; Mareeswaran, P.M.; Lu, K.-L.; Rajagopal, S. Sensitized Near-Infrared Luminescence From Nd^{III}, Yb^{III} and Er^{III} Complexes by Energy-Transfer From Ruthenium 1,3-Bis([1,10]Phenanthroline-[5,6-d]-Imidazol-2-yl)Benzene. *J. Fluoresc.* **2013**, *23*, 1167–1172. [[CrossRef](#)]
31. Forster, T. Energiewanderung und Fluoreszenz. *Naturwissenschaften* **1946**, *33*, 166–175. [[CrossRef](#)]
32. Dexter, D.L. A Theory of Sensitized Luminescence in Solids. *J. Chem. Phys.* **1953**, *21*, 836–850. [[CrossRef](#)]
33. Lazarides, T.; Sykes, D.; Faulkner, S.; Barbieri, A.; Ward, M.D. On the Mechanism of d–f Energy Transfer in Ru^{II}/Ln^{III} and Os^{II}/Ln^{III} Dyads: Dexter-Type Energy Transfer Over a Distance of 20 Å. *Chem.—A Eur. J.* **2008**, *14*, 9389–9399. [[CrossRef](#)]
34. Carneiro Neto, A.N.; Teotonio, E.E.S.; de Sá, G.F.; Brito, H.F.; Legendziewicz, J.; Carlos, L.D.; Felinto, M.C.F.C.; Gawryszewska, P.; Moura, R.T., Jr.; Longo, R.L.; et al. Modeling Intramolecular Energy Transfer in Lanthanide Chelates: A Critical Review and Recent Advances. In *Handbook on the Physics and Chemistry of Rare Earths*; Bünzli, J.-C.G., Pecharsky, V.K., Eds.; Elsevier: Amsterdam, The Netherlands, 2019; Volume 56, pp. 55–162. ISBN 9780444642998.
35. Shyichuk, A.; Câmara, S.S.; Weber, I.T.; Neto, A.N.C.; Nunes, L.A.; Lis, S.; Longo, R.L.; Malta, O.L. Energy transfer upconversion dynamics in YVO₄:Yb³⁺, Er³⁺. *J. Lumin.* **2016**, *170*, 560–570. [[CrossRef](#)]
36. Malta, O. Mechanisms of non-radiative energy transfer involving lanthanide ions revisited. *J. Non-Cryst. Solids* **2008**, *354*, 4770–4776. [[CrossRef](#)]
37. Carneiro Neto, A.N.; Moura, R.T.; Shyichuk, A.; Paterlini, V.; Piccinelli, F.; Bettinelli, M.; Malta, O.L. Theoretical and Experimental Investigation of the Tb³⁺ → Eu³⁺ Energy Transfer Mechanisms in Cubic A₃Tb_{0.90}Eu_{0.10}(PO₄)₃ (A = Sr, Ba) Materials. *J. Phys. Chem. C* **2020**, *124*, 10105–10116. [[CrossRef](#)]
38. Trannoy, V.; Neto, A.N.C.; Brites, C.D.S.; Carlos, L.D.; Serier-Brault, H. Engineering of Mixed Eu³⁺/Tb³⁺ Metal-Organic Frameworks Luminescent Thermometers with Tunable Sensitivity. *Adv. Opt. Mater.* **2021**, *9*, 2001938. [[CrossRef](#)]
39. Malta, O. Ligand—Rare-earth ion energy transfer in coordination compounds. A theoretical approach. *J. Lumin.* **1997**, *71*, 229–236. [[CrossRef](#)]
40. E Silva, F.R.; Malta, O. Calculation of the ligand–lanthanide ion energy transfer rate in coordination compounds: Contributions of exchange interactions. *J. Alloys Compd.* **1997**, *250*, 427–430. [[CrossRef](#)]
41. Neto, A.N.C.; Moura, R.T.; Malta, O.L. On the mechanisms of non-radiative energy transfer between lanthanide ions: Centrosymmetric systems. *J. Lumin.* **2019**, *210*, 342–347. [[CrossRef](#)]
42. Gomez, G.E.; Marin, R.; Neto, A.N.C.; Botas, A.M.P.; Ovens, J.; Kitos, A.A.; Bernini, M.C.; Carlos, L.D.; Soler-Illia, G.J.A.A.; Murugesu, M. Tunable energy transfer process in heterometallic MOFs materials based on 2,6-naphthalenedicarboxylate: Solid-state lighting and near-infrared luminescence thermometry. *Chem. Mater.* **2020**, *32*, 7458–7468. [[CrossRef](#)]
43. Neto, A.N.C.; Mamontova, E.; Botas, A.M.P.; Brites, C.D.S.; Ferreira, R.A.S.; Rouquette, J.; Guari, Y.; Larionova, J.; Long, J.; Carlos, L.D. Rationalizing the Thermal Response of Dual-Center Molecular Thermometers: The Example of an Eu/Tb Coordination Complex. *Adv. Opt. Mater.* **2021**, *10*, 2101870. [[CrossRef](#)]
44. Lyubov, D.M.; Neto, A.N.C.; Fayoumi, A.; Lyssenko, K.A.; Korshunov, V.M.; Taydakov, I.V.; Salles, F.; Guari, Y.; Larionova, J.; Carlos, L.D.; et al. Employing three-blade propeller lanthanide complexes as molecular luminescent thermometers: Study of temperature sensing through a concerted experimental/theory approach. *J. Mater. Chem. C* **2022**, *10*, 7176–7188. [[CrossRef](#)]
45. Ramalho, J.F.C.B.; Dias, L.M.S.; Fu, L.; Botas, A.M.P.; Carlos, L.D.; Neto, A.N.C.; André, P.S.; Ferreira, R.A.S. Customized Luminescent Multiplexed Quick-Response Codes as Reliable Temperature Mobile Optical Sensors for eHealth and Internet of Things. *Adv. Photonics Res.* **2021**, *3*, 2100206. [[CrossRef](#)]
46. Cantuel, M.; Bernardinelli, G.; Imbert, D.; Bünzli, J.-C.G.; Hopfgartner, G.; Piguet, C. A kinetically inert and optically active Cr^{III} partner in thermodynamically self-assembled heterodimetallic non-covalent d–f podates. *J. Chem. Soc. Dalton Trans.* **2002**, *9*, 1929–1940. [[CrossRef](#)]
47. Carnall, W.T.; Crosswhite, H.; Crosswhite, H.M. *Energy Level Structure and Transition Probabilities in the Spectra of the Trivalent Lanthanides in LaF₃*; Argonne: Lemont, IL, USA, 1978.

48. Edvardsson, S.; Klintonberg, M. Role of the electrostatic model in calculating rare-earth crystal-field parameters. *J. Alloys Compd.* **1998**, *275*, 230–233. [[CrossRef](#)]
49. Silver, B.L. *Irreducible Tensor Methods*; ACADEMIC PRESS, INC.: London, UK, 1976; ISBN 0-12-643650-9.
50. Judd, B.R. *Operator Techniques in Atomic Spectroscopy*; McGraw-Hill Book Company: New York, NY, USA, 1998; ISBN 9780691604275.
51. Neto, A.N.C.; Moura, R.T., Jr. Overlap integrals and excitation energies calculations in trivalent lanthanides 4f orbitals in pairs Ln-L (L = Ln, N, O, F, P, S, Cl, Se, Br, and I). *Chem. Phys. Lett.* **2020**, *757*, 137884. [[CrossRef](#)]
52. Moura, R.T., Jr.; Neto, A.N.C.; Aguiar, E.C.; Santos-Jr., C.V.; de Lima, E.M.; Faustino, W.M.; Teotonio, E.E.; Brito, H.F.; Felinto, M.C.; Ferreira, R.A.; et al. (INVITED) JOYSpectra: A web platform for luminescence of lanthanides. *Opt. Mater. X* **2021**, *11*, 100080. [[CrossRef](#)]
53. Carneiro Neto, A.N.; Moura, R.T., Jr.; Coelho, J.A.A.; Silva-Junior, M.E.; Costa, J.L.; Malta, O.L.; Longo, R.L. A Tutorial Review on the Nonradiative Energy Transfer Rates between Lanthanide Ions. *Chin. J. Lumin.* **2022**, *43*, 20. [[CrossRef](#)]
54. Miyakawa, T.; Dexter, D.L. Phonon Sidebands, Multiphonon Relaxation of Excited States, and Phonon-Assisted Energy Transfer between Ions in Solids. *Phys. Rev. B* **1970**, *1*, 2961–2969. [[CrossRef](#)]
55. Golesorkhi, B.; Taarit, I.; Bolvin, H.; Nozary, H.; Jiménez, J.-R.; Besnard, C.; Guénée, L.; Fürstenberg, A.; Piguet, C. Molecular light-upconversion: We have had a problem! When excited state absorption (ESA) overcomes energy transfer upconversion (ETU) in Cr(III)/Er(III) complexes. *Dalton Trans.* **2021**, *50*, 7955–7968. [[CrossRef](#)]
56. Rohatgi, A. WebPlotDigitizer 2021. Available online: <https://automeris.io/WebPlotDigitizer/> (accessed on 6 September 2022).
57. Judd, B.R. Optical Absorption Intensities of Rare-Earth Ions. *Phys. Rev.* **1962**, *127*, 750–761. [[CrossRef](#)]
58. Ofelt, G.S. Intensities of Crystal Spectra of Rare-Earth Ions. *J. Chem. Phys.* **1962**, *37*, 511–520. [[CrossRef](#)]
59. Smentek, L.; Kezdziorski, A. Efficiency of the energy transfer in lanthanide-organic chelates; spectral overlap integral. *J. Lumin.* **2010**, *130*, 1154–1159. [[CrossRef](#)]
60. Milos, M.; Kairouani, S.; Rabaste, S.; Hauser, A. Energy migration within the 2E state of Cr³⁺. *Coord. Chem. Rev.* **2008**, *252*, 2540–2551. [[CrossRef](#)]
61. Dexpert-Ghys, J.; Auzel, F. Existence of cooperative absorption lines for Yb-(OH,OD) pairs: Absolute oscillator strengths. *J. Chem. Phys.* **1984**, *80*, 4003–4012. [[CrossRef](#)]
62. Donega, C.D.M.; Meijerink, A.; Blasse, G. Vibronic transition probabilities in the excitation spectra of the Pr³⁺ ion. *J. Phys. Condens. Matter.* **1992**, *4*, 8889–8902. [[CrossRef](#)]
63. Yamada, N.; Shionoya, S.; Kushida, T. Phonon-Assisted Energy Transfer between Trivalent Rare Earth Ions. *J. Phys. Soc. Jpn.* **1972**, *32*, 1577–1586. [[CrossRef](#)]
64. Fonger, W.; Struck, C. Unified model of energy transfer for arbitrary Franck-Condon offset and temperature. *J. Lumin.* **1978**, *17*, 241–261. [[CrossRef](#)]
65. Auzel, F.; De Sa', G.; de Azevedo, W. An example of concentration sensitive electron-phonon coupling in {(C₄H₉)₄N}₃EuxY_{1-x}(NCS)₆ and a new hypothesis for self-quenching. *J. Lumin.* **1980**, *21*, 187–192. [[CrossRef](#)]
66. Blasse, G. Luminescence of inorganic solids: From isolated centres to concentrated systems. *Prog. Solid State Chem.* **1988**, *18*, 79–171. [[CrossRef](#)]
67. Nie, W.; Boulon, G.; Monteil, A. Vibronic levels and zero-phonon lines of Cr³⁺-doped yttrium aluminium garnet (Y₃Al₅O₁₂). *J. Phys.* **1989**, *50*, 3309–3315. [[CrossRef](#)]
68. Silverstein, R.M.; Webster, F.X.; Kieml, D.J. *Spectrometric Identification of Organic Compounds*, 7th ed.; John Wiley & Sons: New York, NY, USA, 2005; ISBN 0-471-39362-2.
69. Reinhard, C.; Güdel, H.U. High-Resolution Optical Spectroscopy of Na₃[Ln(dpa)₃]·13H₂O with Ln = Er³⁺, Tm³⁺, Yb³⁺. *Inorg. Chem.* **2002**, *41*, 1048–1055. [[CrossRef](#)]
70. Costa, I.F.; Blois, L.; Carneiro Neto, A.N.; Teotonio, E.E.S.; Brito, H.F.; Carlos, L.D.; Felinto, M.C.F.C.; Moura, R.T., Jr.; Longo, R.L.; Faustino, W.M.; et al. Reinterpreting the Judd–Ofelt Parameters Based on Recent Theoretical Advances. In *Luminescent Materials: Fundamentals and Applications*; Brik, M.G., Srivastava, A.M., Eds.; De Gruyter: Berlin, Germany, 2023; pp. 19–62.

Disclaimer/Publisher's Note: The statements, opinions and data contained in all publications are solely those of the individual author(s) and contributor(s) and not of MDPI and/or the editor(s). MDPI and/or the editor(s) disclaim responsibility for any injury to people or property resulting from any ideas, methods, instructions or products referred to in the content.